PUBLISHED BY INSTITUTE OF PHYSICS PUBLISHING AND SISSA
RECEIVED: *February 24, 2006*
ACCEPTED: *March 20, 2006*
PUBLISHED: *April 10, 2006*

Application of a new procedure for design of 325 MHz RFQ*

P.N. Ostroumov†, V.N. Aseev and A.A. Kolomiets

Argonne National Laboratory,
9700 S. Cass Avenue, Argonne, IL, 60439, U.S.A.
E-mail: ostroumov@phy.anl.gov

ABSTRACT: A new procedure for designing Radio Frequency Quadrupole (RFQ) accelerators has been developed. We present an integrated RFQ design procedure, which is based on modern three-dimensional field map calculations and beam dynamics simulations. The design procedure was integrated with the beam dynamics design and simulation codes DESRFQ & TRACK and applied to the development of a 325 MHz RFQ capable of delivering a 2.5 MeV H^- beam with 40 mA peak current for the proton driver (PD) at Fermi National Accelerator Laboratory (FNAL).

KEYWORDS: Accelerator modelling and simulations (multi-particle dynamics; single-particle dynamics); Acceleration cavities and magnets superconducting (high-temperature superconductor; radiation hardened magnets; normal-conducting; permanent magnet devices; wigglers and undulators); Instrumentation for particle accelerators and storage rings - low energy (linear accelerators, cyclotrons, electrostatic accelerators)

* This work was supported by the U.S. Department of Energy under Contracts No. W-31-109-ENG-38.
† Corresponding author.

2006 JINST 1 P04002

Contents

1. RFQ specifications for the FNAL Proton Driver

Similar to many other linear accelerators, the PD [1] requires an RFQ for initial acceleration and formation of the bunched beam structure. The required parameters of the FNAL RFQ are very similar to the SNS [2] and J-PARC [3]. The RFQ design includes two main tasks: a) the beam dynamics design resulting in a vane tip modulation table for machining and b) the resonator electromagnetic design resulting in the final dimensions of the resonator. The focus of this paper is on the first task. Initial RFQ design specifications are given in table 1. The PD RFQ will operate at 325 MHz and the acceleration of ~40 mA pulsed current is considered a relatively moderate problem in the physics design of the RFQ. The design of the RFQ, MEBT and whole PD lattice has been iterated several times to satisfy more advanced RFQ beam specifications. Particularly, the longitudinal phase space beam emittance must be halo free to avoid excessive beam loss in the high energy section of the PD.

Broad RFQ design and construction experience suggests that RFQs operating above 200 MHz can be based on 4-vane structures. For RFQs longer than ~3λ, where λ is the

	Parameter	Value
1	Input Energy, keV	50
2	Output Energy, MeV	2.5
3	Accelerated beam current, mA	40
4	Peak surface field, kV/cm	≤330
5	Total length of the vanes, m	~3
6	Acceleration efficiency, %	>95
7	Input rms transverse emittance, normalized, π mm mrad	0.25
8	Transverse rms emittance growth factor	<1.1
9	Longitudinal rms emittance, π keV·deg	≤150
10	Axial-symmetric output beam	yes

Table 1. Initial specifications for the RFQ design.

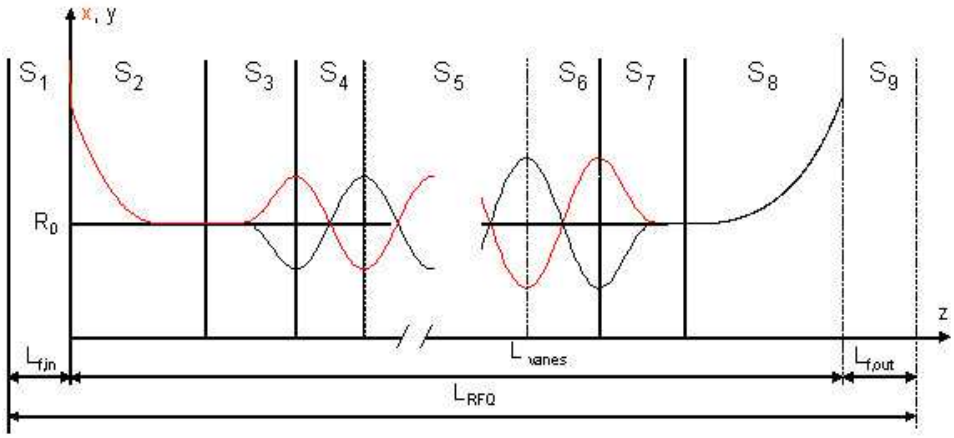

Figure 1. Side view of typical RFQ vane profiles. S_1 is the fringe field region with the length $L_{f,in}$; S_2 is the input radial matcher, S_3 is the input transition cell, S_4 is the first accelerating cell, S_5 is the section with regular accelerating cells, S_6 is the last accelerating cell, S_7 is the output transition cell, S_8 is the output radial matcher, S_9 is the fringe field region with the length $L_{f,out}$.

rf wavelength, it is difficult to stabilize the operating field and damp field errors. To address this problem, the SNS and J-PARC RFQ designs included π-mode stabilizing loops (PISLs) [3]. PISLs complicate the resonator design and increase its cost, therefore we propose to minimize the length of the RFQ resonator to allow for the use of field stabilizers simpler than PISLs. For example, field stabilization with longitudinal rods installed at the endwalls was successfully applied to several RFQs (see, for example, [4]).

2. Design procedure

We assume that the reader is familiar with RFQ fundamental properties as is given in references [5],[6]. For the beam dynamics design, the RFQ is divided into three main sections: an input radial matcher, a main modulated vane section where bunching and acceleration occur, and an output radial matcher.

The main section of the RFQ is designed using the code DESRFQ [7]. This code uses a Laplace equation solver, which takes into account the physical vane shape as described in the next subsection, to generate the RFQ vane tip geometry in every cell and the RFQ parameters required for the final simulations with the TRACK [8] or PARMTEQ [9] codes. The TRACK code tracks particles through the whole RFQ in 3D accounting for both the external and internal space charge fields. The 3D electric field in the regular bunching-accelerating section has been presented by an 8-term Fourier-Bessel expansion. These terms are the same as in the PARMTEQ code [9].

2.1 Shape of the vane tips

An RFQ vane can be divided to several functional sections and we distinguish between the nine different sections of the vanes as is shown in figure 1.

Modulation of the vanes in the regular accelerating section is shown in figure 2. The following notation is used in this figure and the following text. R_0 is the RFQ average radius or distance from the axis to the vane tip at the cross section with exact quadrupole symmetry, R_e is the vane tip curvature radius in the transverse plane, $L_i \approx \beta\lambda/2$ is the distance between the points with exact quadrupole symmetry for *i-th* half-period of modulation (HPM) as was

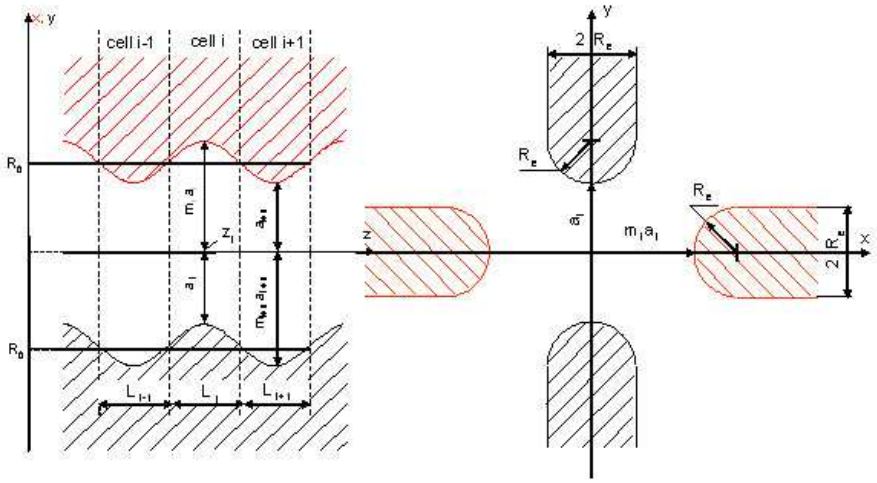

Figure 2. Side view of the vane profiles (on the left) and cross-section of the modulated vanes.

introduced in [10], $m = \frac{2R_0}{a} - 1$ is the modulation factor, and a is the aperture. We apply simple sinusoidal vane modulations keeping R_0 and R_e constant along the RFQ. The distance from axis to the modulated vane tip surface along the i-th HPM is

$$x_t(z) = R_0\left[1 \pm \frac{m_i - 1}{m_i + 1}\cos\left(\frac{\pi}{L_i}(z - Z_i)\right)\right]$$
$$y_t(z) = R_0\left[1 \mp \frac{m_i - 1}{m_i + 1}\cos\left(\frac{\pi}{L_i}(z - Z_i)\right)\right], Z_i - \frac{L_i}{2} \le z \le Z_i + \frac{L_i}{2} \quad (1)$$

where z is the longitudinal coordinate along the vanes, Z_i is the longitudinal coordinate of the center of the *i-th* HPM. The upper signs are applied when the horizontal vane has a maximal distance *ma* and vertical vane has a minimal distance *a* from the z-axis in the center of the *i-th* HPM. As is shown in figure 1, we also use the standard definition of the accelerating cells [5],[6]. For example, ray-tracing of particles in the simulation code is performed through the accelerating cells.

2.2 Peak surface field

Peak surface field E_s is the most important initial parameter of the RFQ design. The choice of the peak surface field can be based on the broad operational experience of RFQs. Using the Kilpatrick limit, $\boldsymbol{E_{KP}}$, is a common way of evaluating the peak tolerable surface fields in RFQs. However, there are discrepancies in the definition of the Kilpatrick limit in the literature and in many cases the Kilpatrick limit is calculated without taking into account the gap between the electrodes. The code DESRFQ calculates Kilpatrick limit using the following equation:

$$gE_{KP}^3\left(1 - \exp\left(\frac{-48.6E_{KP}}{gf^2}\right)\right) = 1.8 \cdot 10^5 \exp\left(\frac{170}{E_{KP}}\right) \quad (2)$$

where $\boldsymbol{E_{KP}}$ [kV/cm] is the Kilpatrick limit of the peak surface field, $\boldsymbol{f}$ [MHz] is the operational frequency, $\boldsymbol{g}$ [cm] is the minimum distance between unmodulated RFQ electrodes and is defined as

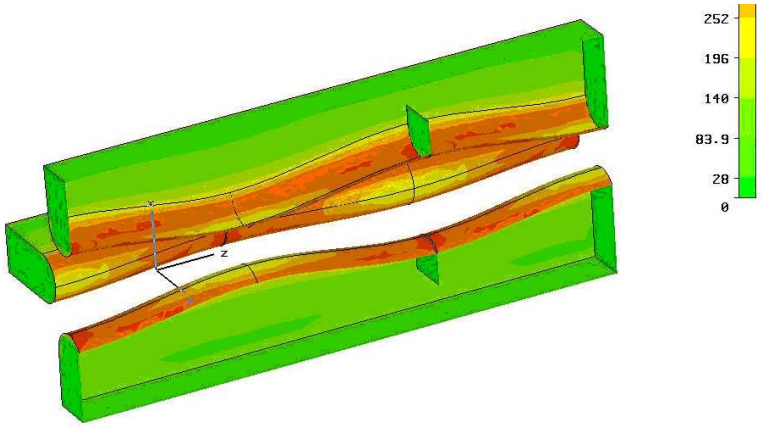

Figure 3 Cut-out view of the EMS model of the RFQ electrodes at $\beta = 0.0481$, $m = 1.98$.

$$g = R_0\left(\sqrt{2}\left(1+\frac{R_e}{R_0}\right)-2\frac{R_e}{R_0}\right). \tag{3}$$

The Kilpatrick limit obtained from (2) and (3) reflects the results of D.W. Kilpatrick's original work [11].

The results of peak surface field calculations by the code DESRFQ have been compared with the simulations performed using CST Electro-Magnetic Studio (EMS) [12]. These simulations have been carried out for several cells with different modulation factors and lengths. The EMS model of one of the cells is shown in figure 3 and the surface field along the vane tip in the cross-section with exact quadrupole symmetry is shown in figure 4. For comparison, we provide a table of peak surface fields calculated for the 90.45 kV design voltage in different cells along the RFQ using three different codes (see table 2). Table 3 shows the Fourier-Bessel expansion coefficients for one of the cells obtained using these codes. One can see excellent consistency between the codes, especially for the acceleration efficiency A_{01} and focusing term A_{10}.

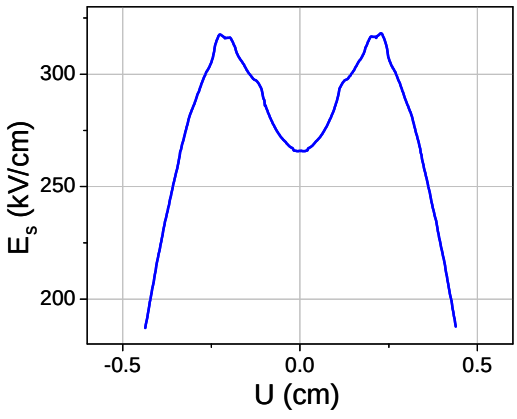

Figure 4. Electric field on the electrode surface in the cross-section with the exact quadrupole symmetry of the model shown in figure 3. U is the path length along the vane tip surface in the XY plane.

Cell number	DESRFQ	PARMTEQ	EM studio
74	331.7	356.5	333.5
150	331.0	350.8	328.3
223	332.1	341.5	317.6

Table 2. Peak fields (kV/cm) in the different cells along the RFQ.

Coefficients of field expansion	CST EM studio simulation	Ref. [13]	DESRFQ
A_{01}	0.949	0.941	0.951
A_{03}	0.019	0.021	0.015
A_{10}	0.602	0.601	0.602
$A_{12}I_4(kR_0)$	0.056	0.063	0.056
$A_{21}\ I_2(2kR_0)$	-0.019	-0.014	-0.020
$A_{23}\ I_6(2kR_0)$	-0.019	-0.007	-0.020
$A_{30}\ I_0(3kR_0)$	-0.011	-0.010	-0.011
$A_{32}\ I_4(3kR_0)$	-0.010	0.003	-0.009

Table 3. Field expansion coefficients obtained by different codes.

2.3 Design of the bunching-accelerating section

The first design step is the choice of the average radius R_0, which can be found using the code DESRFQ. Figure 5 shows the phase advance σ and the modulus of the Floquet function ρ [14] as a function of the average radius calculated for a fixed peak field of $E_s = 1.8E_{KP}$ and $R_e = 0.75R_0$ for unmodulated vanes. Once the average radius is known, the cell-to-cell RFQ parameters and the vane modulation law are generated using the DESRFQ code.

The next step is the multi-particle simulations with the code TRACK. This procedure has been repeated to reach optimum compromise between the following four conflicting requirements: 1) forming low longitudinal emittance, 2) avoiding transverse rms emittance growth, 3) maximizing beam transmission, and 4) maximizing the accelerating rate. Conditions 1 and 2 can be satisfied at a relatively low amplitude of the accelerating field (small modulation) while the conditions 3 and 4 require a higher modulation at initial bunching. The final RFQ vane modulation and synchronous phase as a function of the cell number are given in figure 6.

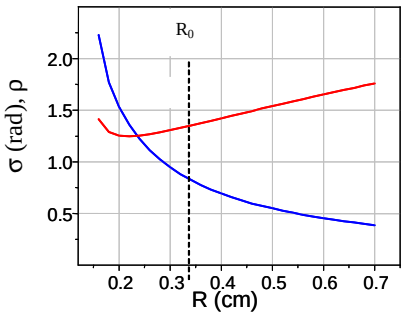

Figure 5. The transverse phase advance (the blue curve) and modulus of the Floquet function (the red curve).

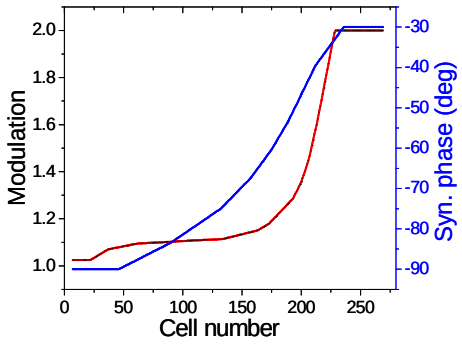

Figure 6. Modulation factor (the red curve) and synchronous phase (the blue curve) as a function of cell number.

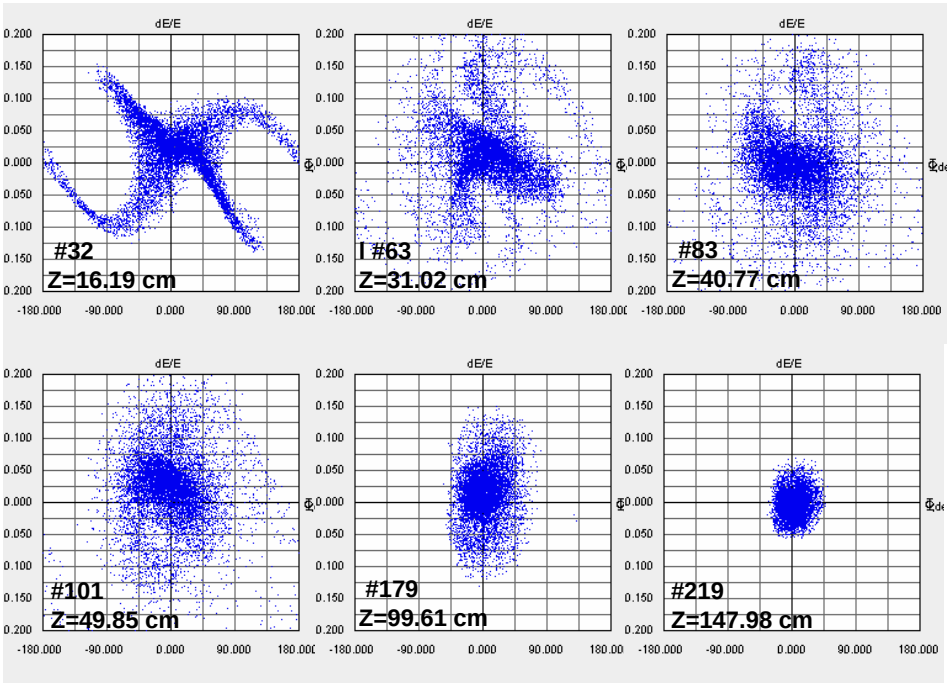

Figure 7. Phase space plots in the longitudinal phase plane along the RFQ.

For stable particle motion in the longitudinal phase space the amplitude of the accelerating field must be sufficient to compensate space charge forces. If this condition is applied in the bunching section there are two consequences: a) the RFQ forms large longitudinal emittance, and b) a rapid increase of peak current of the bunch results in transverse mismatch and emittance growth. Therefore in our design the accelerating field is slightly lower than necessary to provide stable longitudinal motion in the presence of space charge forces. However, the condition of the lack of stability in the longitudinal phase plane takes place over a short distance. Therefore, it helps to create a uniform distribution to fill the stability area in the following cells. Figure 6 shows the evolution of the phase space plots in the longitudinal phase space along the RFQ. The particle distribution in the cell #32 (figure 7) is a typical example of the lack of stability for some fraction of particles. The beam space charge increases the energy spread and ultimately uniformly fills the stability area provided by increased longitudinal focusing in the downstream cells.

The space charge effect on transverse motion is described by parameter ***h,*** introduced in [5] as:

$$h = \frac{\lambda}{\sigma_0 I_0} \frac{I\,B}{\beta\gamma^2 \varepsilon_n} \tag{4}$$

where I is the beam average current, B is the bunching factor, σ_0 is the phase advance of transverse oscillations for zero current, ε_n is the transverse normalized emittance, and I_0 is the characteristic current defined by the expression:

$$I_0 = 4\pi\varepsilon_0 \frac{A m_0 c^3}{eZ}.$$

$I_0 = 3.13 \cdot 10^7$ A for protons. The matched beam size in the presence of space charge must be increased according to the expression:

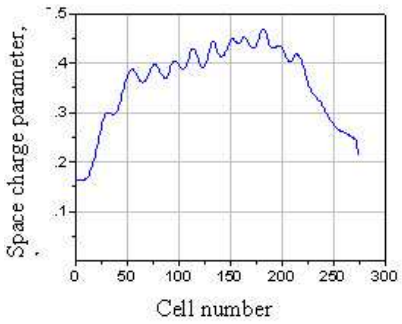

Figure 8. The space charge parameter evolution along the RFQ.

$$R_{env}(h) = R_{env}(0)\sqrt{h+\sqrt{1+h^2}} \tag{5}$$

while the phase advance is equal to:

$$\sigma(h) = \sigma_0\,(\sqrt{1+h^2} - h) \tag{6}$$

According to expression (4), to keep the space charge parameter constant along the RFQ and to avoid excessive space charge effects, the bunching factor *B* must be proportional to the beam velocity β. However, this condition is difficult to satisfy, especially if the total length of the RFQ is minimized. The space charge parameter along the PD RFQ for a 45 mA peak injected beam current is shown in figure 8. The space charge parameter reaches its maximum value h_{max} = 0.46 at the end of the bunching section, this results in a 25% envelope size increase and a 36% tune depression.

Table 4 presents the final RFQ parameters. The transverse phase advance remains high along the RFQ and reflects the strong suppression of the space charge forces.

2.4 Input radial matcher and transition cell

In the input radial matcher section (RMS) the distance from the axis to the vane tip is a function of the longitudinal coordinate and is given by the expression

$$\begin{aligned} x_t(z) = y_t(z) &= \frac{R_0}{\cos\left(\dfrac{\pi(\kappa D - z)}{2D}\right)}, \quad 0 \le z \le \kappa D \\ x_t(z) = y_t(z) &= R_0, \quad \kappa D \le z \le L_{RMS} \end{aligned} \tag{7}$$

Average radius R_0, cm	0.340
Vane curvature radius R_e, cm	0.255
Inter-vane voltage U_0, kV	90.45
Vane length, cm	302.428
Modulation factor	1.0 to 2.0
Synchronous phase, degree	-90 to -30
Transverse phase advance, 0 (45 mA), degree	~45(32)
Normalized transverse acceptance, π mm·mrad	2.89
Peak surface field, kV/cm	330
Peak surface field, Kilpatrick units	1.8

Table 4. Basic RFQ parameters.

Injected peak current, mA		0	10	20	30	45
Twiss parameters	α	1.90	2.10	2.34	2.60	3.0
	β, cm/rad	7.90	8.03	8.64	9.28	10.6
Mismatch factor		1.021	1.025	1.031	1.038	1.051

Table 5. Beam rms input parameter and dynamic mismatch factor.

where D is the length of an 'ideal' matcher with an infinite electrode profile, and $L_{RMS} = \kappa D$ is the matcher length where $\kappa = 12/13$ defines the electrode cutoff. The RFQ design procedure includes an optimization of the geometry parameter D which is equal to $D = 3.8$ cm for the proposed PD RFQ. The matched Twiss parameters for different input beam currents are given in table 5. Twiss parameters are calculated upstream of the vanes at a distance equal to $L_{f,in}$.

For the final beam dynamics simulations the 3D fields in the input matcher section have been generated using EMS. Figure 9 shows the vane configuration of the radial matcher in EMS. To include fringe fields in the TRACK code, the simulations starts at a distance $L_{f,in} = \beta_{in}\lambda$ upstream of the vane's flat end (see figure 1), where β_{in} is the injected beam velocity.

A transition cell is located between the input radial matcher and the first accelerating cell. The geometry of this cell is designed following K.R. Crandall [15]. The distance from the axis to the electrodes is given by the expressions:

$$x_t(z) = y_t(z) = R_0 \quad , \; 0 \le z \le L_T - L$$

$$x_t(z) = R_0\left(1 \pm \frac{m_1 - 1}{m_1 + 1}C(z)\right), y_t(z) = R_0\left(1 \mp \frac{m_1 - 1}{m_1 + 1}C(z)\right), \; L_T - L \le z \le L_T \;, \tag{8}$$

$$\text{where} \;\; C(z) = \frac{3}{4}\cos\left(\frac{\pi(L_T - z)}{2L}\right) + \frac{1}{4}\cos\left(\frac{3\pi(L_T - z)}{2L}\right),$$

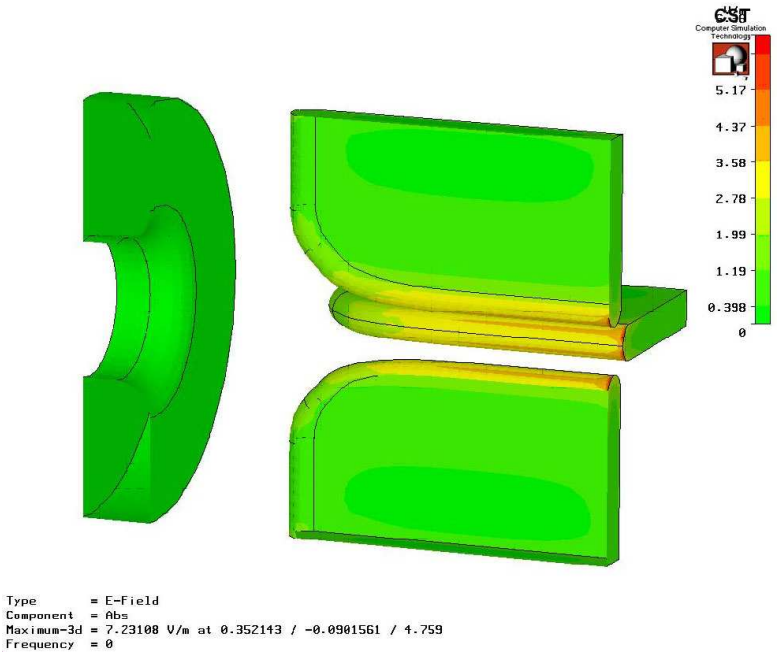

Figure 9. Cut out view of the input radial matcher in the EMS window.

L_T is the length of the transition cell and $L = \sqrt{0.75} L_T$. The upper signs are applied when the horizontal vane has a maximum displacement $m_1 a_1$ and the vertical vane has a minimum displacement a_1 from the axis at the end of the transition cell. Figure 1 shows the profile of the transition cell.

2.5 Output radial matcher and transition cell

The output radial matcher is designed to form an axially-symmetric beam exiting the RFQ. The shape of the output matcher as well as the transition cell is similar to the input radial matcher with mirror reflection. The distance *r(z)* from the axis to the electrode in the output radial matcher as a function of the longitudinal coordinate is given by the expression:

$$x_t(z) = y_t(z) = R_0 \quad , \quad 0 \le z \le L$$
$$x_t(z) = y_t(z) = \frac{R_0}{\cos\left(\frac{\pi(z-L)}{2D}\right)} \quad , \quad L \le z \le L_{RMS} \tag{9}$$

where L = 1.55 cm is the length of the matcher section with constant aperture $x_t(z) = y_t(z) = R_0$, and D = 10.75 cm. The parameters L and D have been optimized to provide an axially-symmetric beam. The output transition cell is located between the last accelerating cell and the output RMS and its geometry is defined from the expressions:

$$x_t(z) = R_0\left(1 \pm \frac{m_N - 1}{m_N + 1}\tilde{C}(z)\right), \qquad y_t(z) = R_0\left(1 \mp \frac{m_N - 1}{m_N + 1}\tilde{C}(z)\right), \qquad 0 \le z \le L$$
$$x_t(z) = y_t(z) = R_0, \qquad L \le z \le L_T \tag{10}$$
$$\text{where } \tilde{C}(z) = \frac{3}{4}\cos\left(\frac{\pi z}{2L}\right) + \frac{1}{4}\cos\left(\frac{3\pi z}{2L}\right)$$

with the same parameters as in (8). The upper signs are applied when the horizontal vane has a maximum displacement $m_N a_N$ and the vertical vane has a minimum displacement a_N from the axis at the upstream end of the transition cell. In the TRACK simulations we use the 3D field distribution calculated with the EMS software. The EMS cut out view of the output radial matcher is shown in figure 10. We have extracted 3D fields inside the vanes and over the distance $L_{f,out} = L_{f,in}$ outside of the vanes to include fringe fields. The fringe fields vanish over the distance $L_{f,out}$ from the flat ends of the vanes.

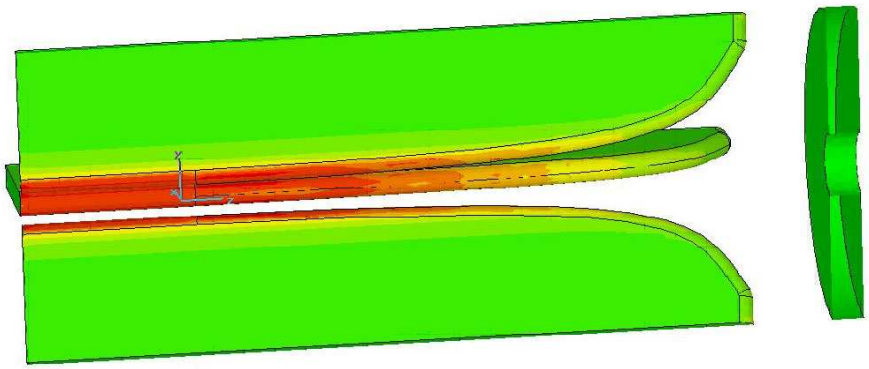

Figure 10. Cut out view of the output radial matcher in the EMS window.

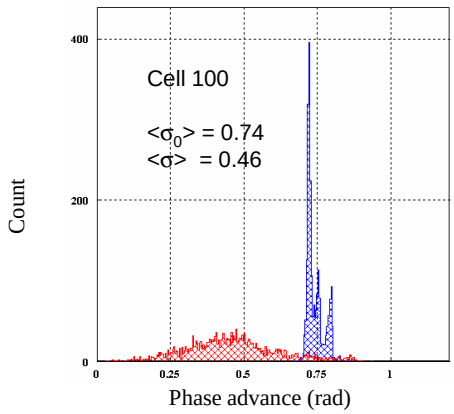

Figure 11. Transverse phase advances of particles calculated for I = 0 (blue) and I = 45 mA (red).

3. Beam dynamics simulations

The multi-particle simulations of the RFQ beam dynamics were performed using the TRACK code. Particle motion in a realistic RFQ field is nonlinear and the most comprehensive beam dynamics studies can be carried out by numerical simulations. Useful information reflecting the nonlinear particle motion can be obtained from the analysis of particle trajectories. As an example, figure 11 shows histograms of phase advances or transverse oscillation frequencies averaged over the focusing period of individual particles in the transverse phase space calculated for zero beam current and for the beam current I = 45 mA in cell #100 where the space charge parameter is close to its maximum value. The shift in the average value of the distribution is in exact agreement with expression (6). In addition to the shift of average value, the picture shows significant dispersion of the distribution due to nonlinear space charge fields and the coupling of transverse and longitudinal motion. Accumulation of particles close to zero phase advance is a sign of halo formation in the transverse phase space. The shape of the distribution shown in figure 11 is still acceptable and indicates a negligible halo formation for the given beam current. As is seen from the distribution, there are no particles with zero frequency (or zero phase advance). Further increase of the beam current results in a higher number of particles near the stability border and a higher emittance growth rate. This effect is clearly seen from figure 12 and figure 13 which show transverse rms emittance growth and

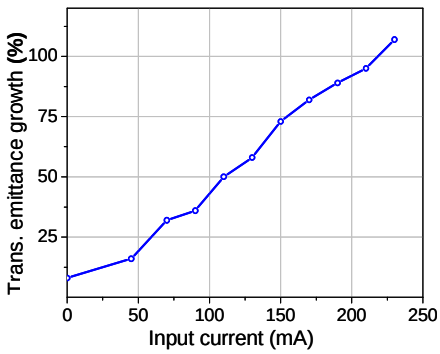

Figure 12. Transverse rms emittance at the cell #172 as a function of input beam current.

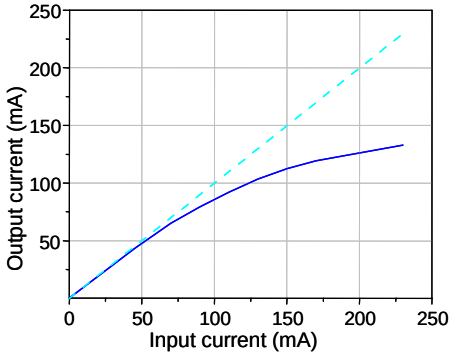

Figure 13. Transmission through the RFQ calculated for the same input transverse emittance.

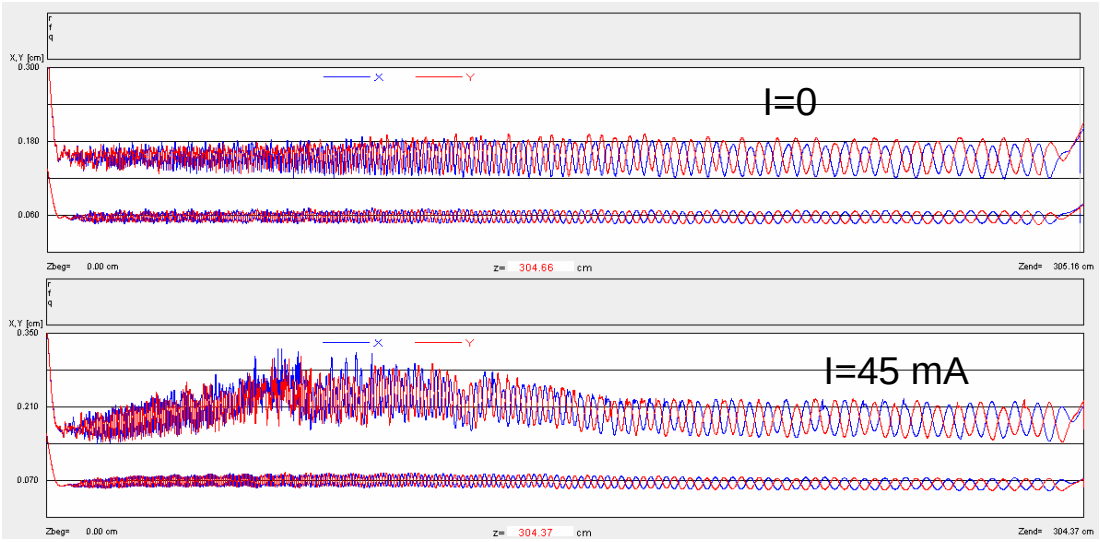

Figure 14. Beam envelopes along RFQ simulated by the TRACK code. The pair of lower curves are beam rms sizes, the upper curves are beam envelopes in X- and Y- planes shown in different colours.

output beam current as a function of the input beam current. The simulations have been carried out assuming that the input emittance is a constant independent of the beam current.

Beam envelopes calculated by the TRACK code are shown in figure 14. The rms envelope for the design beam current reaches its maximum at the end of bunching section as predicted by expression (6). The beam envelope growth along the bunching section reflects some beam halo formation. Further envelope growth is limited by the aperture and particle losses. Despite some halo formation, the total particle losses do not exceed 2%. Most particles are lost in the cells with a large space charge parameter as is seen from figure 15.

The proposed design of the RFQ is capable of efficiently accelerating high current beams, which can be seen in figure 13. The current limit of the proposed RFQ can be estimated to be around 140 mA.

After several iterations between DESRFQ and TRACK simulations the design of the RFQ has been fixed and we performed simulations for a million particles using the TRACK code. The field distribution in the end regions including transition cells was obtained using the EMS code. In the regular accelerating section the field is calculated using either 2-term or

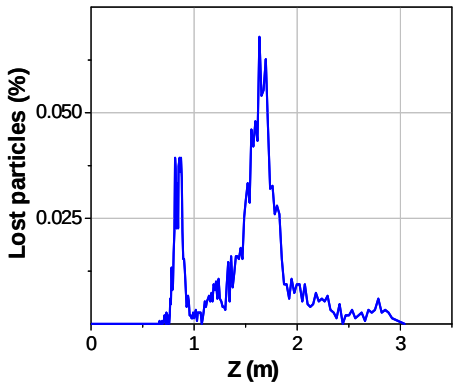

Figure 15. Relative beam losses in the RFQ as a function of the distance along the RFQ.

Parameter	2-term potential	8-term potential
Output energy, MeV/u	2.498	2.498
Transverse emittance, rms, in/out, π mm mrad	0.100/0.100	0.100/0.102
Transverse emittance, 99.5%, in/out, π mm mrad	0.139/0.176	0.139/0.171
Long. emittance, rms, keV/u deg	137	133
Long. emittance, 99.5%, keV/u deg	1870	1870
Transmission efficiency, %	98.4	97.8
Acceleration efficiency, %	96.4	95.9
Particle losses inside the RFQ, %	1.6	2.2

Table 6. Beam parameters at the exit of the RFQ.

8-term Fourier-Bessel field expansion. The expansion coefficients have been obtained from DESRFQ as described above. We provide both 2-term and 8-term results for comparison in table 6. Simulation with the 8-term potential shows slightly higher losses and lower transmission as expected.

The emittance and profile of the beam exiting the RFQ obtained from simulation of 10^6 particles are shown in figure 16. The rms and total longitudinal emittances are 133 and 5265 π keV/u·deg correspondingly. There is no beam halo and the phase space distribution is Gaussian as is seen from figure 17. Twiss parameters of the beam exiting the RFQ are shown in table 7 for several different injection currents. The Twiss parameters are calculated over the distance $L_{f,out}$ downstream of the vane end.

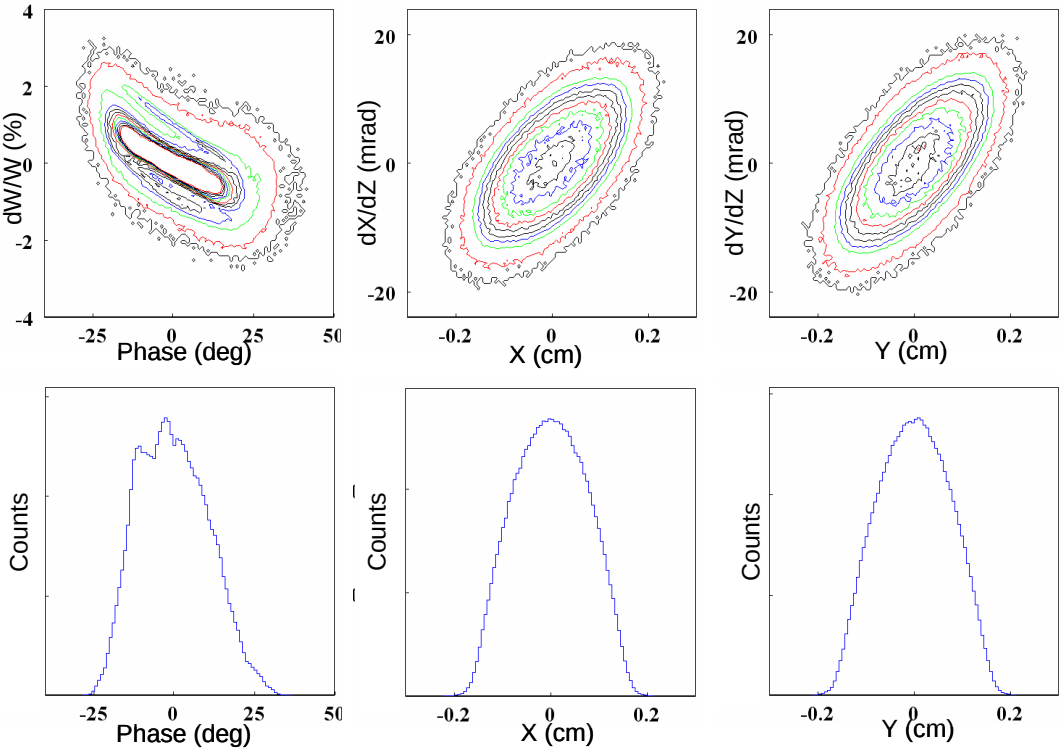

Figure 16. Phase space plots (on the top) and beam profiles of the accelerated beam. The outermost isoline contains 100% of particles, the next isoline contains 99% of particles.

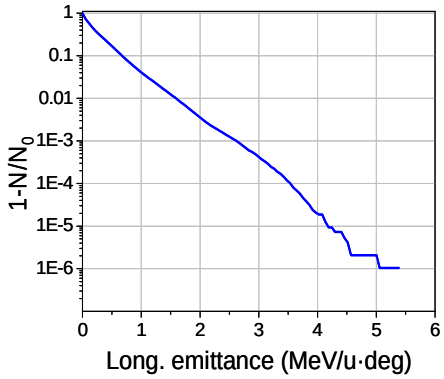

Figure 17. Fraction of particles outside of the given emittance as a function of the longitudinal emittance.

Input beam current (mA)	Twiss parametrs			
	X plane		Y plane	
	α	β	α	β
0	-0.56	0.013	-0.72	0.013
10	-0.65	0.0148	-0.77	0.0146
20	-0.70	0.0144	-0.83	0.0143
30	-0.78	0.0155	-0.88	0.0151
45	-0.78	0.0159	-0.88	0.0155

Table 7. Twiss parameters of the beam exiting the RFQ.

4. Conclusion

A procedure has been developed for the physics design of high-intensity RFQs. The procedure is a modification of previously known RFQ design concepts unified with new entirely three-dimensional codes for the design and simulation of the RFQ beam dynamics. For a moderate beam current of ~40 mA, there is no transverse emittance growth, the longitudinal emittance is low and there is no non-Gaussian beam halo. For the FNAL Proton Driver application one of the main design criteria was to keep the RFQ length short to avoid complicated stabilizing tuners. A simple two-dimensional vane cut provides a high degree of linearity to the particle motion in the RFQ.

References

[1] G.W. Foster and J.A. MacLachlan, *A Multi-mission 8 GeV injector Linac as a Fermilab booster replacement*, in *Proc. of the LINAC-2002*, p. 826.
[2] A. Ueno, *Proc. of LINAC-2004*, Monterey, CA, 2000, p. 545.
[3] A. Ratti et al., *Conceptual design of the SNS RFQ*, in *Proc. of the LINAC 98*, p. 276.
[4] T.S. Bhatia et al., *Proc. of the PAC 1991*, p. 1884.
[5] I.M. Kapchinskii and V.A. Teplvakov, *Prib. Tekh. Eksp.* **2** (1970) 19;
Prib. Tekh. Eksp. **4** (1970) 17.
[6] J. Staples, *RFQ's: an introduction*, LBNL Technical Report, LBL-29472, 1990.
[7] A.A. Kolomiets, *The code DESRFQ*, ITEP/ANL, Technical note, 2005.
[8] P.N. Ostroumov, V.N. Aseev and B. Mustapha, *Beam loss studies in high-intensity heavy-ion Linacs*, *Phys. Rev. ST. Accel. Beams*, **7** (2004) 090101.

[9] K.R. Crandall et al., *RFQ design codes*, Los Alamos National Laboratory report LA-UR-96-1836. (Revised May 20, 1998).
[10] L. Root, *Beam dynamics of the finalized ISAC RFQ*, Design Note, TRI-DN-ISAC-97, 1997, Vancouver, Canada.
[11] W.D. Kilpatrick, *Rev. Scient. Instrum.*, **28**, No. 10 (1957) 824.
[12] CST Electromagnetic Studio, *User manual version 2.0*, January 2004, CST GmbH, Darmstadt, Germany http://www.cst.de/.
[13] K.R. Crandall, *LANL report*, LA-9695-MS, UC-28, April 1983.
[14] M. Reiser, *Theory and design of charged particle beams*. John Wiley & Sons, Inc., 1994.
[15] K.R. Crandall, *Proc. of the LINAC-1994*, p. 227.